International Journal of Nanomedicine

Dovepress
open access to scientific and medical research

Open Access Full Text Article

ORIGINAL RESEARCH

Crafting Docetaxel-Loaded Albumin Nanoparticles Through a Novel Thermal-Driven Self-Assembly/Microfluidic Combination Technology: Formulation, Process Optimization, Stability, and Bioavailability

Juan Du[1,*], Li-Li Shi[2,*], Wei-Wei Jiang[3], Xue-Ai Liu[3], Xin-Hong Wu[3], Xiang-Xiang Huang[3], Ming-Wei Huo[3], Ling-Zhi Shi[3], Jingjian Dong[2], Xiaohong Jiang[2], Renyu Huang[4], Qing-Ri Cao[3], Wenzhou Zhang[1]

[1]Department of Pharmacy, The Affiliated Cancer Hospital of Zhengzhou University & Henan Cancer Hospital, Zhengzhou, 450008, People's Republic of China; [2]College of Medicine, Jiaxing University, Jiaxing, People's Republic of China; [3]College of Pharmaceutical Sciences, Soochow University, Suzhou, 215123, People's Republic of China; [4]College of Social Science, Soochow University, Institute of Culture and Tourism Development, Soochow University, Suzhou, 215123, People's Republic of China

*These authors contributed equally to this work

Correspondence: Wenzhou Zhang, Department of Pharmacy, The Affiliated Cancer Hospital of Zhengzhou University & Henan Cancer Hospital, Zhengzhou, 450008, People's Republic of China, Email hnzzzwzx@sina.com; Qing-Ri Cao, College of Pharmaceutical Sciences, Soochow University, 199 Ren-Ai Road, Suzhou Industrial Park, Jiangsu, 215123, People's Republic of China, Email qrcao@suda.edu.cn

Background: The commercial docetaxel (DTX) formulation causes severe side effects due to polysorbate 80 and ethanol. Novel surfactant-free nanoparticle (NP) systems are needed to improve bioavailability and reduce side effects. However, controlling the particle size and stability of NPs and improving the batch-to-batch variation are the major challenges.

Methods: DTX-loaded bovine serum albumin nanoparticles (DTX-BSA-NPs) were prepared by a novel thermal-driven self-assembly /microfluidic technology. Single-factor analysis and orthogonal test were conducted to obtain the optimal formulation of DTX-BSA-NPs in terms of particle size, encapsulation efficiency (EE), and drug loading (DL). The effects of oil/water flow rate and pump pressure on the particle size, EE, and DL were investigated to optimize the preparation process of DTX-BSA-NPs. The drug release, physicochemical properties, stability, and pharmacokinetics of NPs were evaluated.

Results: The optimized DTX-BSA-NPs were uniform, with a particle size of 118.30 nm, EE of 89.04%, and DL of 8.27%. They showed a sustained release of 70% over 96 hours and an increased stability. There were some interactions between the drug and excipients in DTX-BSA-NPs. The half-life, mean residence time, and area under the curve (AUC) of DTX-BSA-NPs increased, but plasma clearance decreased when compared with DTX.

Conclusion: The thermal-driven self-assembly/microfluidic combination method effectively produces BSA-based NPs that improve the bioavailability and stability of DTX, offering a promising alternative to traditional formulations.

Keywords: DTX-BSA nanoparticles, thermal-driven self-assembly, microfluidic technology, in-vitro release, pharmacokinetics

Introduction

Docetaxel (DTX) is a first-generation taxane drug that shows good efficacy in the treatment of advanced breast cancer, ovarian cancer, and non-small cell lung cancer.[1–3] A commercially available formulation contains nonionic surfactant polysorbate 80 and ethanol as co-solvent to overcome the challenge posed by the limited solubility of DTX. However, this formulation has been found to be associated with notable adverse effects, including cumulative hypersensitivity reactions, fluid retention, nausea, and peripheral neuropathy.[4] Therefore, novel efficient and surfactant-free alternative formulations for DTX must be developed.

Received: 9 February 2024
Accepted: 16 May 2024
Published: 1 June 2024

Graphical Abstract

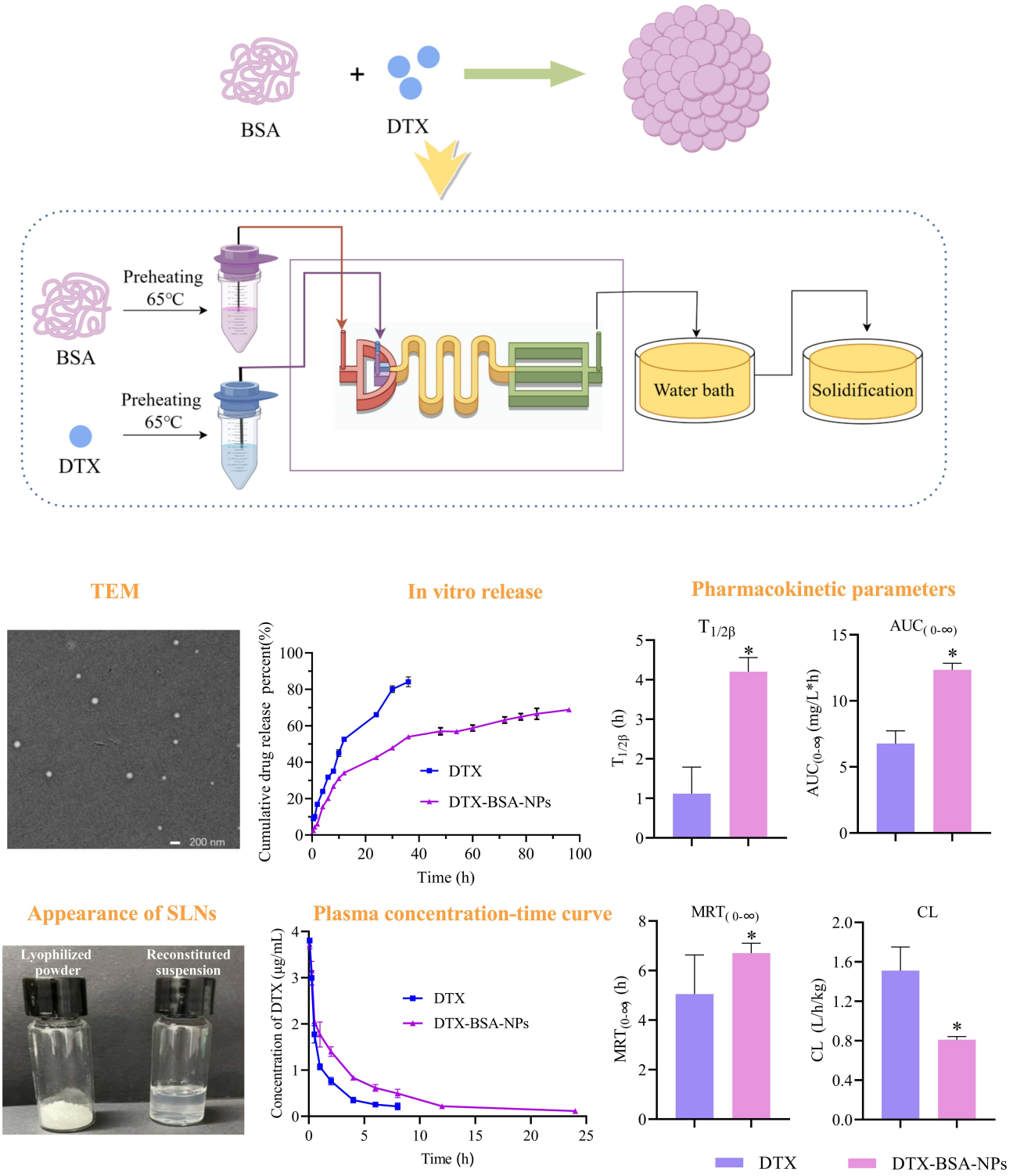

Nanoparticle (NP) drug delivery systems, with advantages such as improvement of drug solubility, passive targeting to tumor, and prolonged circulation time, have risen as a hot topic of research.[5–8] Researchers have developed various dosage forms, including polymeric micelles, liposomes, solid lipid NPs, and biomimetic NPs, for encapsulating DTX to enhance its efficient delivery to tumor tissues.[9–11]

Among them, albumin attracts increasing attention and has become an effective drug delivery platform owing to its excellent biocompatibility, nontoxicity, non-immunogenic properties, and biodegradability.[12–14] Recent studies have shown that albumin has the ability to target tumor tissue by binding to the highly expressed albumin receptor gp60 and cysteine-rich acidic secretory protein (SPARC) in tumor tissue.[15,16] Albumin-bound paclitaxel (Abraxane) was prepared by NP albumin bound (Nab) technology, a patented novel nanotechnology developed by Abraxis BioScience (CA, USA), and approved by the FDA in 2005 for the treatment of breast cancer.[17–19] Subsequently, it was approved for the treatment of lung cancer[20,21] and pancreatic cancer.[22] This breakthrough has brought great benefits to patients with cancer and provided new insights for researchers in the field of nanomedicine, highlighting the remarkable role of albumin NPs in antitumor therapy and other treatments. Currently, the most commonly used proteins are human serum albumin (HSA) and bovine serum albumin (BSA). However, given the exorbitant cost and limited availability of HSA, BSA is considered a suitable alternative carrier.

BSA NPs can be prepared through various techniques, including emulsification,[23,24] nano-spray drying,[25,26] Nab technique,[27] and heat-driven self-assembly.[28] Among them, self-assembly is based on exposing or altering hydrophobic regions on the surface or inside the protein. By heating denaturation or adding reducing agents to open the disulfide bond inside the protein, drug molecules can interact with the hydrophobic region of the protein and promote self-assembly of albumin NPs.[29] Some reports showed that the albumin NPs prepared by this method have uniform particle size, high encapsulation efficiency (EE), and strong drug loading (DL) ability. Furthermore, unlike other preparation methods, heat-driven self-assembly eliminates the need for certain organic solvents, such as chloroform and ethyl acetate; crosslinking agents, such as glutaraldehyde; and surfactants such as polysorbate 80 and polyvinyl alcohol.[30,31] The utilization of these substances could potentially compromise the biological activity of therapeutic agents. Therefore, BSA NPs prepared using heat driven self-assembly possess the advantages of minimizing toxic side effects and ensuring excellent safety profiles. However, controlling the particle size and stability of BSA NPs and improving the batch-to-batch variation in the industrial sites are the major challenges in the preparation of BSA NPs.[28,29,32,33]

Microfluidics, also known as lab-on-A-chip technology, originated from the concept of "Miniaturized Total Analysis Systems" (μTAS) proposed by Manz et al in 1990.[34] It refers to the manipulation of minute volumes of fluids (ranging from picoliters to microliters) and the separation of micro-scale samples by utilizing microchannels (with dimensions ranging from tens to hundreds of micrometers) or microfluidic chips. In recent years, the interest in utilizing microfluidic technology for drug delivery systems involving NPs has been increasing. Various applications, including droplets, emulsions, microcapsules, microparticles, and NPs, have been explored.[35–40] The implementation of microfluidic technology in the production of nanoscale formulations has significantly improved the limitations of traditional methods. These improvements include achieving consistent particle sizes, enhanced reproducibility, better sample dispersion, and increased EE.[41–44] Consequently, this technological advancement has provided a robust platform for driving industrial research in the field of nanoscale formulation development.

On the basis of the above background, DTX-BSA-NPs were prepared by combining thermal-driven self-assembly and microfluidic technology. Three main factors affecting the particle size and EE of DTX-BSA-NPs were identified by a single factor test for thermal-driven self-assembly. Then, the optimized formulation was obtained by orthogonal test through comparing the particle size and EE. Furthermore, for the DTX-BSA-NPs prepared by the combination method, the effect of oil/water flow rate and pump pressure on the particle size, EE, and DL was investigated to optimize the preparation process. The stability of the final NPs was studied under stress and accelerated conditions. The relative bioavailability of DTX-BSA-NPs was compared with that of DTX in SD rats. This study is of great importance for the advancement and exploration of the novel technology of albumin NPs.

Experimental Section

Materials

Docetaxel (DTX) was purchased from Xi'an Natural Field Bio-Technique Co., Ltd (Xi'an, China). The commercial DTX formulation was purchased from Hangzhou Sanofi Pharmaceutical Co., Ltd (Hangzhou, China). Bovine serum albumin (BSA) was purchased from Beijing Solarbio Science & Technology Co., Ltd (Beijing, China). Sodium Gluconate was purchased from energy chemical Co., Ltd. $Na_2HPO_4{\cdot}12H_2O$ was purchased from SIGMA-ALDRICH® Co., Ltd (Shanghai, China). Tris buffer was purchased from BBI Life Sciences Co., Ltd (Shanghai, China). All other chemicals used were of analytical grade.

Preparation of DTX-BSA-NPs by Thermal-Driven Self-Assembly

DTX-BSA-NPs were prepared using heat-driven self-assembly as described below. In brief, BSA was dissolved in buffer solution to form an aqueous phase. DTX was dissolved in ethanol to obtain an organic phase. Both phases were preheated at 65°C for 5 min in a water bath. The DTX solution was then slowly injected into the BSA solution by using a syringe, followed by incubation at 65°C for some minutes. Subsequently, the solutions were transferred to a 50 mM sodium gluconate solution, and the resulting mixture was immediately placed in an ice-water bath and allowed to stand for 5 min. The unencapsulated DTX was further removed through ultrafiltration.

The experimental design was divided into two main parts. First, a single-factor experiment was conducted, which involved factors such as the mass ratio of DTX to BSA (1:7, 1:9, 1:11), concentrations of DTX (20, 15, 10, and 5 mg/mL) and BSA (45, 22.5, 9, and 4.5 mg/mL), incubation temperature (60°C, 65°C, 70°C, and 75°C) incubation time (3, 10, 15, and 30 min), BSA buffer solution (phosphate-buffered saline [PBS], 12% disodium hydrogen phosphate, and 20 mM Tris; pH 8.0), and BSA preheating (yes or no). Second, an orthogonal experimental design (L_9 [3^3]) was employed to establish the optimal formulation and preparation process for DTX-BSA-NPs on the basis of the results of the single-factor study.

Preparation of DTX-BSA-NPs by Thermal-Driven Self-Assembly/ Microfluidic Combination Technology

DTX ethanol solution (5.0 mg/mL) and BSA solution (22.5 mg/mL, in 20 mM Tris buffer) were preheated at 65°C in a water bath. In addition, 25 mL of 50 mM sodium gluconate and 50 mL ultrapure water were also preheated at the same temperature. The DTX and BSA solutions were pumped into the microchannel reactor at a predetermined flow rate to mix together, and the resulting mixture was incubated in a water bath at 65°C for 3 min, followed by transferring into 25 mL of 50 mM sodium gluconate. Afterwards, it was thoroughly mixed and cooled in an ice water bath for 5 min to obtain stable DTX-BSA-NPs. The detailed flowchart is shown in Figure 1.

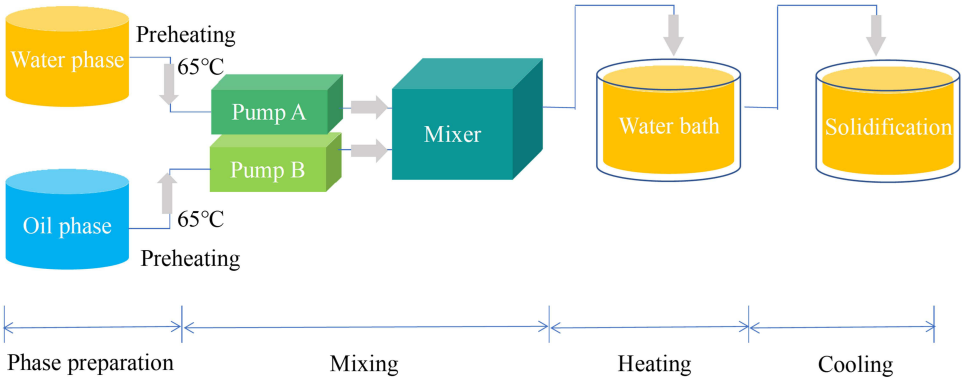

Figure 1 Flow chart of the preparation process of DTX-BSA-NPs through a microfluidic technology.

In this experiment, the primary factors influencing the formation of DTX-BSA-NPs were investigated through a single-factor study. The flow rate of the microfluidic pump and system pressure were individually optimized to obtain optimal DTX-BSA-NPs in terms of particle size, EE, and DL.

The DTX-BSA-NPs were placed in a 10 mL centrifuge tube and freeze-dried for 48 h to obtain DTX-BSA-NP powder.

Measurement of Particle Size

The particle size of DTX-BSA-NPs were evaluated using a HPP 5001 dynamic light scattering instrument (Malvern, UK) and a NICOMP TM 380 ZLS (NICOMP, USA). Prior to measurement, the samples were appropriately diluted in distilled water.

Determination of EE and DL Capacity

EE and DL were determined using ultrafiltration. NP suspension (1 mL) was added to an ultrafiltration tube, followed by centrifugation at 3500 rpm for 15 min. The unencapsulated drug was calculated by analyzing the drug concentration in the filtrate obtained after centrifugation. The total drug amount was determined by dissolving the NP suspension in acetonitrile to release the encapsulated DTX. EE was determined by dividing the amount of drug encapsulated within the NPs by the total amount of DTX used, and DL capacity was calculated as the ratio of the drug content encapsulated within the NPs to the polymer content as follows:

$$\mathrm{EE} = \frac{\mathrm{W}_{\text{total DTX}} - \mathrm{W}_{\text{unencapsulated DTX}}}{\mathrm{W}_{\text{total DTX}}} \times 100\%$$

$$\mathrm{DL} = \frac{\mathrm{W}_{\text{total DTX}} - \mathrm{W}_{\text{unencapsulated DTX}}}{\mathrm{W}_{\text{total DTX}} + \mathrm{W}_{\text{polymer}}} \times 100\%$$

Reproducibility of Preparation Process

In accordance with the optimal preparation process of DTX-BSA-NPs by using thermal-driven self-assembly/microfluidic combination technology, three batches of samples were prepared to investigate the reproducibility of the preparation process. The particle size, size distribution, EE, and DL of DTX-BSA-NPs were measured to investigate the repeatability and reliability of the results.

Three batches of freeze-dried samples were prepared. The freeze-dried samples were redissolved in deionized water, and the particle size, particle-size distribution, EE, and DL were determined.

pH Measurement of DTX-BSA-NPs

The pH of DTX-BSA-NPs was determined in accordance with the Chinese Pharmacopoeia 2020 edition. DTX-BSA-NPs (5 mL) were placed in a 15 mL centrifuge tube. The electrode was rinsed three times with ultrapure water and then dried with a wiping paper before immersing it into the test solution. Once the pH reading stabilized, the data were recorded.

Transmission Electron Microscopy (TEM)

The morphology of DTX-BSA-NPs were observed through TEM (Tecnai G220, FEI, USA). The samples were diluted for 200 times. Twenty microliters of the dilution was placed on copper grids with films, dried under an infrared lamp, and then viewed under the transmission electron microscope.

Differential Scanning Calorimetry (DSC)

The DSC spectra of DTX; BSA; physical mixture of DTX, BSA, and sodium gluconate; and DTX-BSA-NPs were characterized by DSC (Model 2010, TA Instruments, USA). In brief, each sample was placed in aluminum pans and heated at a scanning rate of 10°C/min from 40°C to 300°C under dry nitrogen gas purge.

Fourier Transform Infrared (FTIR) Spectroscopy

The FTIR spectra of DTX; BSA; physical mixture of DTX, BSA, and sodium gluconate; and DTX-BSA-NPs were characterized using an FTIR spectrophotometer (Model Excaliber Series UMA-500, Bio-Rad, USA). The wavelength ranged from 500 cm^{-1} to 4000 cm^{-1} with 2 cm^{-1} resolution.

In-vitro Release

In-vitro release of DTX-BSA-NPs was carried out using dynamic membrane dialysis. PBS (100 mL, pH 7.4) containing 0.1% (v/v) polysorbate 80 was used as the release medium to ensure sink conditions. In brief, DTX and DTX-BSA-NPs (equivalent to 2 mg DTX) were dispersed in 2 mL release medium and carefully positioned inside pre-treated dialysis bags. These dialysis bags were then placed in the release medium and vibrated in a water bath at 37°C. At time intervals of 0.5, 1, 2, 4, 6, 8, 10, 12, 24, 30, 36, 48, 54, 60, 72, 78, 84, and 96 h, 500 μL of the samples was withdrawn and replaced with fresh medium. After being filtered through a 0.22 μm filter membrane, the samples were injected into the high-performance liquid chromatography (HPLC) system to determine peak areas. The average cumulative drug release percentage was calculated at each time point (n = 3) to generate an in-vitro cumulative release profile for DTX-BSA-NPs.

Stability Study

In accordance with the guidelines set forth in the 2015 edition of the Chinese Pharmacopoeia, stress and accelerated tests were used to compare the stability of commercial DTX formulation (0.5 mL, 20 mg) and freeze-dried DTX-BSA-NPs. The conditions of the stress test include high temperature (60°C ± 2°C), high humidity (92.5 ± 5% relative humidity [RH]), and strong illumination (4500 ± 500 Lx). Commercial DTX formulation (0.5 mL, 20 mg) was diluted with sterile saline to 10 mg/mL. The diluted DTX solution and freeze-dried DTX-BSA-NPs were stored under stress conditions. Samples were taken on the 0th, 5th 10th, 15th, and 30th days to observe and determine the changes in the appearance, redispersibility, pH, and drug content of DTX and freeze-dried DTX-BSA-NPs. For the accelerated test, samples were enclosed in a sealed container and exposed to either 25°C/65% RH or 40°C/65% RH conditions. At specific time intervals (1, 2, and 3 months), samples were taken to determine the changes in the appearance, redispersibility, pH, and content of DTX and freeze-dried DTX-BSA-NPs.

Pharmacokinetic Study

Animal Study

A total of 10 male Sprague–Dawley rats (200–250 g, Shanghai, China) were employed for the in-vivo pharmacokinetic study, with random allocation into two groups (n = 5, per group). All experiments were approved by the Institutional Animal Care and Use Committee of Soochow University and followed National Institutes of Health guide for the care and use of laboratory animals. Prior to the experiment, all rats underwent a fasting period of 12 h while being provided unrestricted access to water. DTX and DTX-BSA-NPs were diluted with deionized water to a concentration of 10 mg/mL and administered via intravenous injection at a dosage of 5 mg DTX/kg of body weight. Blood samples (approximately 0.5 mL) were collected from the orbital venous plexus at specified intervals, including 0, 5, 15, and 30 min and 1, 2, 4, 6, 8, 12, and 24 h post-dosing. Subsequently, the obtained blood samples were centrifuged at 12,000 ×g for 3 min. The resulting plasma samples were transferred to new glass tubes and stored at −20°C until analysis.

Treatment of Plasma Samples

Each plasma sample (100 μL) was mixed with 300 μL PTX (4.0 μg/mL) solution as an internal standard (IS). Ether (1 mL) was added to the mixture and then agitated for 5 min by using a vortex mixer. The organic phase was transferred into a tube and evaporated with nitrogen on a water bath at 40°C. The residue was reconstituted with 0.2 mL acetonitrile and fully mixed. After centrifugation at 12,000 rpm for 3 min, 20 μL of the supernatant was injected into the HPLC system.

HPLC Conditions

Chromatographic separation was conducted using an HPLC instrument (Thermo Fisher U3000) with a flow rate of 1.0 mL/min. A ChromCore 120 C_{18} column (4.6 mm ×150 mm, 5 μm) was utilized, and the column temperature was maintained at 25°C. The concentration of DTX was determined at a wavelength of 230 nm. The mobile phase composition consisted of acetonitrile, methanol, and 0.02 M ammonium acetate buffer salt in the ratio of 22:30.5:47.5 (v/v/v%, pH 5.0).

Data Analysis

Pharmacokinetic parameters were calculated using DASver 2.0 pharmacokinetic software. Non-compartmental methods were employed to calculate the pharmacokinetic parameters of DTX. The results were expressed as mean ± standard deviation. Statistical analysis was conducted using ANOVA, with the significance level set at $p < 0.05$ or $p < 0.01$.

Results and Discussion

Effects of Formulation and Process Factors on DTX-BSA-NPs Prepared by Thermal-Driven Self-Assembly

BSA NPs have been extensively investigated for the delivery of anticancer drugs due to their excellent biocompatibility, nontoxicity, non-immunogenicity, biodegradability, and ability to target tumor tissues through specific receptor interactions.[45,46] As a novel organic solvent-free approach to produce albumin NPs,[47] thermal-driven self-assembly was used in the current study to prepare DTX-BSA-NPs.

Single-Factor Experiment

Three different mass ratios (1:7, 1:9, and 1:11) were considered to investigate the effect of mass ratio of DTX to BSA on the particle size, EE, and DL of DTX-BSA-NPs. The results are shown in Figures 2, 3, 2A and 3A. The particle sizes at the three ratios were 99.73 ± 0.31, 122.37 ± 0.90, and 148.57 ± 2.48, respectively. As the BSA ratio increased, the particle size of DTX-BSA-NPs gradually increased. When the mass ratio of DTX to BSA was set at 1:9, the NPs exhibited a relatively higher EE of 84.53 ± 1.18. This finding indicated that the EE of NPs does not have a linear relationship with the DTX-to-BSA mass ratio, aligning with Na Qu's research findings.[48] As shown in Figure 3A, the mass ratio of DTX to BSA had no significant effect on the DL of NPs. Consequently, considering factors such as particle size, EE, and DL, a mass ratio of 1:9 was selected for the following study.

The concentration of BSA may affect the characteristics of DTX-BSA NPs. Various concentrations of BSA (45, 22.5, 9, and 4.5 mg/mL) were investigated, as shown in Figures 2, 3, 2B and 3B. The size of DTX-BSA-NPs varied significantly with decreasing BSA concentration. At 45 mg/mL BSA, the NPs were excessively large, with a size of 190.53 nm. By contrast, at 9 mg/mL BSA, they diminished to a small size of 96.80 nm. Further reducing the BSA concentration to 4.5 mg/mL resulted in an even smaller particle size of 27.37 nm. The results demonstrated that the particle size of the NPs increases with the concentration of BSA, aligning with the findings of some studies.[49,50] During the heat-driven process, peptide chains in the protein unfold, exposing hydrophobic groups. This exposure leads to new intermolecular noncovalent hydrophobic interactions.[51] As a result, an increase in BSA concentration reduces the distance between molecules, facilitating more effective and faster intermolecular interactions.[52] This mechanism ultimately results in the formation of larger NPs. At a BSA concentration of 22.5 mg/mL, the DTX-BSA-NPs exhibited a size of 116.75 nm, an EE rate of 76.81%, and a DL capacity of 8.14%. Consequently, a BSA concentration of 22.5 mg/mL was selected for the following Figures 2, 3, 2C and 3C show that DTX concentration had a significant effect on the properties of NPs. When the DTX concentration was 5 mg/mL, the particle size, EE, and DL of DTX-BSA-NPs were 127.50 nm, 85.23%, and 8.55%, respectively. However, at a DTX concentration of 10 mg/mL, all these parameters decreased, with the particle size measuring 71.82 nm, EE at 73.91%, and DL reduced to 6.94%. At DTX concentrations of 15 and 20 mg/mL, the mixed DTX and BSA solutions presented a white precipitate, indicating that DTX cannot be encapsulated by BSA under high-drug concentration. This phenomenon further prevented the formation of NPs. Considering the above results, a DTX concentration of 5 mg/mL was chosen for the following experiments.

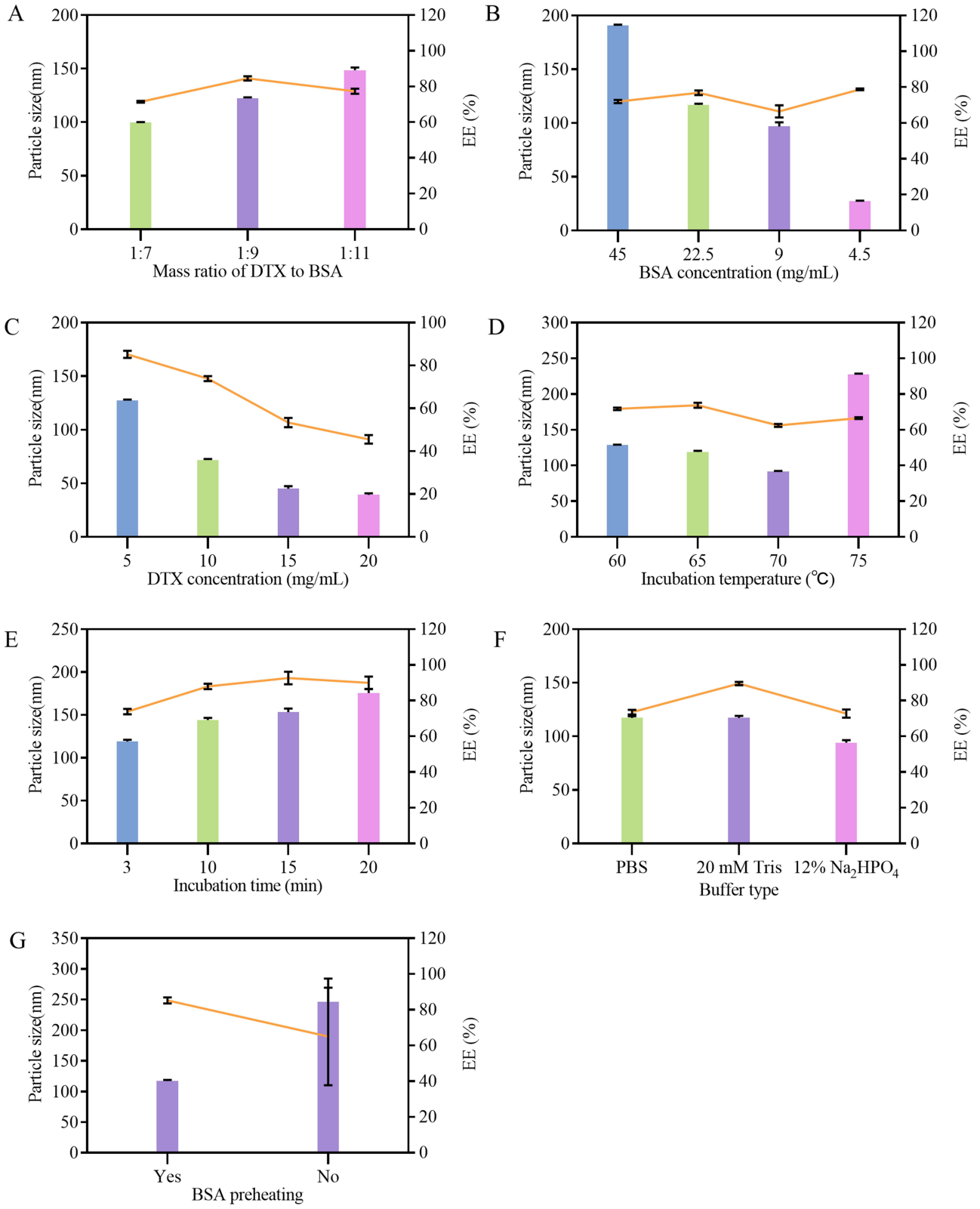

Figure 2 Effects of various factors on the particle size and EE of DTX-BSA-NPs. (**A**) the effect of mass ratio of DTX to BSA. (**B**) the effect of BSA concentration. (**C**) the effect of DTX concentration. (**D**) the effect of incubation temperature. (**E**) the effect of incubation time. (**F**) the effect of different buffer types. (**G**) the influence of preheating BSA. All data are presented as mean±SD (n = 3), with color bars indicating particle size and a line chart displaying EE.

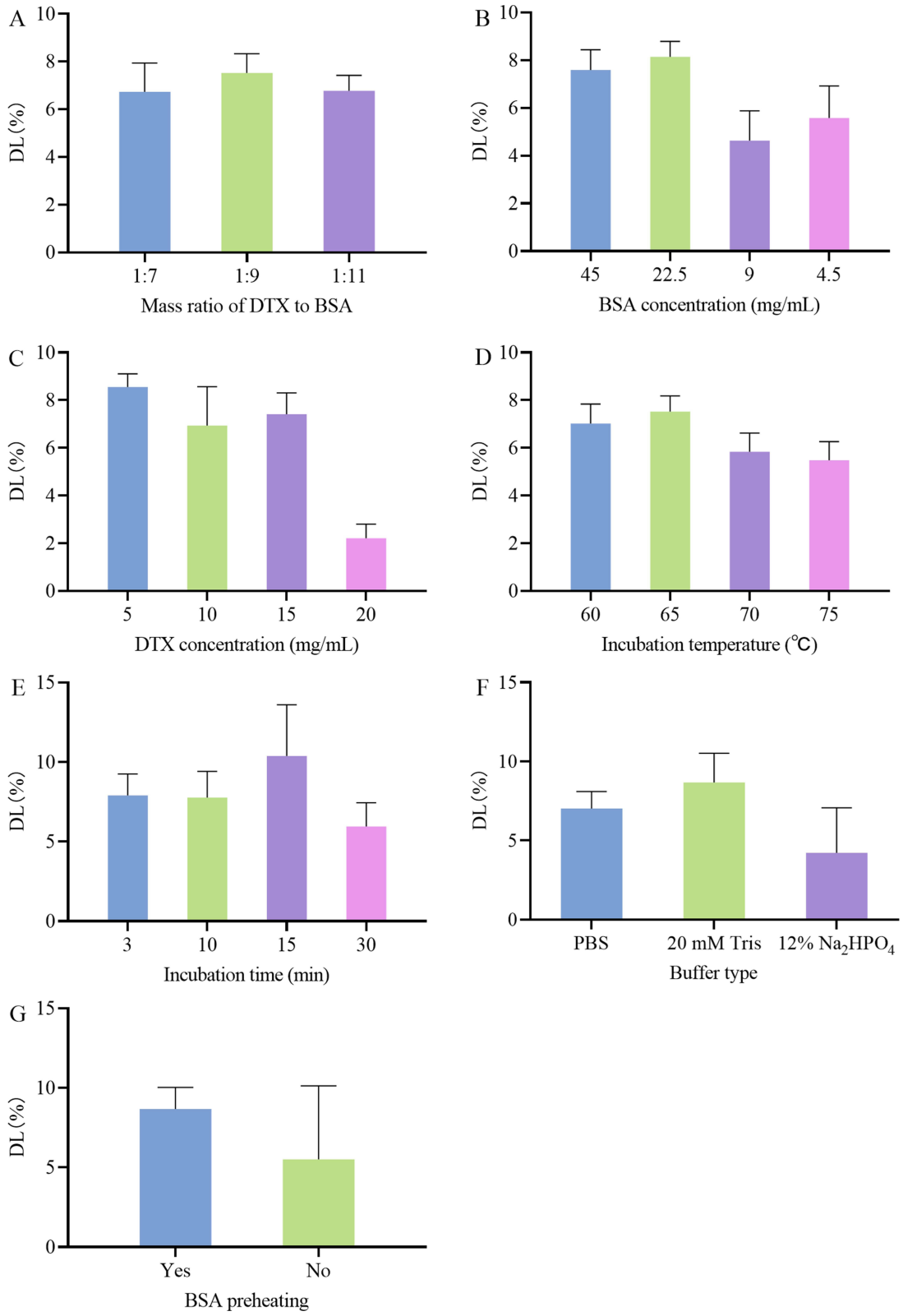

Figure 3 Effects of various factors on the DL of DTX-BSA-NPs. (**A**) the effect of mass ratio of DTX to BSA. (**B**) the impact of BSA concentration. (**C**) the effect of DTX concentration. (**D**) the effect of incubation temperature. (**E**) the impact of incubation time. (**F**) the effect of different buffer types. (**G**) the influence of BSA preheating. All data are presented as mean±SD (n = 3).

Various temperatures were tested in the preparation process to understand the influence of incubation temperature on the properties of DTX-BSA-NPs. The results are presented in Figures 2, 3, 2D and 3D. As the incubation temperature increased, the particle size of DTX-BSA-NPs exhibited remarkable variations. At temperatures of 60°C and 65°C, the DTX-BSA-NPs displayed similar sizes, with mean particle sizes of 128.63 and 119.05 nm, respectively. At 70°C, the particle size decreased to 91.36 nm. However, when the incubation temperature reached 75°C, the particle size of DTX-BSA-NPs increased, probably due to the intense deformation and aggregation of BSA under high-temperature condition.[49] At the temperatures of 60°C and 65°C, the NPs exhibited relatively high EE and DL, with 71.78% ± 0.76% and 73.80% ± 1.4% for EE and 7.02% ± 0.82% and 7.52% ± 0.66% for DL. However, when the temperature increased to 70°C and 75°C, the EE and DL decreased to 62.46 ± 0.8%, 66.58 ± 0.57%, and 5.84 ± 0.78% and 5.48 ± 0.78%, respectively. This trend can be attributed to the rapid thermal aggregation of protein molecules at higher temperatures, which leads to stronger interactions among the protein molecules.[53] This intense interaction potentially reduces the chances for complete encapsulation of DTX. The findings showed relatively higher EE and DL values of 73.80% and 7.52% at an incubation temperature of 65°C. Taking all these findings into consideration, an incubation temperature of 65°C was chosen for the following experiments.

Figures 2, 3, 2E and 3E exhibit the effect of incubation time on the properties of NPs. With an increase in incubation time, the particle size of DTX-BSA-NPs gradually increased, and the EE improved. At an incubation time of 3 min, the particle size of DTX-BSA-NPs was 119.04 nm, which was deemed moderate in size. The EE and DL at this duration reached 73.85% and 7.91%, respectively. Therefore, an incubation time of 3 min was selected for the subsequent experiments.

The stability of proteins is highly dependent on environmental conditions. Buffer condition is one of the main influencing factors.[54] Figures 2, 3, 2F and 3F show the influence of different buffer solutions on the properties of DTX-BSA-NPs. The particle size of DTX-BSA-NPs was nearly identical in PBS and 20 mM Tris buffer solutions, with a suitable size of around 120 nm. However, in the presence of 20 mM Tris buffer solution, the EE and DL of DTX-BSA-NPs reached 89.56% and 8.67%, respectively, showing high drug encapsulation and DL. This finding may be related to the fact that the Tris buffer, with its –OH and amine groups, interacts with BSA through hydrogen bonding, thus stabilizing the protein structure.[55] Consequently, 20 mM Tris solution was chosen as the preferred medium for BSA.

Preheating of BSA solution during the preparation process was considered in this study to check whether it has a considerable effect on the properties of NPs, as shown in Figures 2, 3, 2G and 3G. An increase in particle size up to 246.54 nm was found without preheating, with a remarkably large standard deviation (SD) of particle size. However, when the BSA solution was preheated, the particle size of DTX-BSA-NPs reduced to 117.23 nm, and the EE and DL could reach up to 85.20% and 8.67%, respectively. Consequently, preheating was employed for NP preparation in the following experiments.

Orthogonal Experiment

As different factors can influence the properties of DTX-BSA-NPs, optimizing their formulation and preparation process is essential using a multi-factor design. Considering the results of single-factor experiment, three crucial factors were identified: BSA concentration, DTX concentration, and incubation time. A three-factor and three-level orthogonal experiment was conducted on the basis of the L_9 [3^3] table design to further investigate these factors (Table 1).

Table 1 Three-Factor and Three-Level Design of Orthogonal Test

Level	Factor		
	A (BSA Concentration, mg/mL)	B (DTX Concentration, mg/mL)	C (Incubation Time, Min)
1	45	1	1
2	22.5	5	3
3	9	10	5

Tables 2 and 3 present the results of orthogonal experiments, with particle size and EE as evaluation criteria. From the R-values in Table 2, the order of importance that influenced particle size was determined to be A (BSA concentration) > B (DTX concentration) > C (incubation time). According to the R-values in Table 3, the factors affecting EE in decreasing order of significance were A (BSA concentration) > C (incubation time) > B (DTX concentration). Tables 4 and 5 display the results of variance analysis, with particle size and EE as the evaluation criteria. Regarding the particle size, none of the factors (A, B, or C) showed significant influence. However, in terms of EE, factors A and C demonstrated a significant effect. Therefore, considering all the results from the orthogonal experiments, the optimal

Table 2 Results of Orthogonal Test on Particle Size

Test Number	A BSA Concentration (mg/mL)	B DTX Concentration (mg/mL)	C Incubation Time (min)	Particle Size (nm)
1	1	1	1	320.70
2	1	2	2	232.10
3	1	3	3	246.60
4	2	1	2	131.70
5	2	2	3	112.00
6	2	3	1	59.67
7	3	1	3	322.83
8	3	2	1	35.69
9	3	3	2	34.39
K1	799.40	775.23	416.06	
K2	303.37	379.79	398.19	
K3	392.91	340.66	681.43	
K1-	266.47	258.41	138.69	
K2-	101.12	126.60	132.73	
K3-	130.97	113.55	227.14	
R	165.34	131.81	5.96	

Table 3 Results of Orthogonal Test on EE%

Test Number	A BSA Concentration (mg/mL)	B DTX Concentration (mg/mL)	C Incubation Time (min)	EE (%)
1	1	1	1	82.09
2	1	2	2	91.30
3	1	3	3	79.96
4	2	1	2	95.71
5	2	2	3	87.92
6	2	3	1	80.90
7	3	1	3	75.14
8	3	2	1	77.90
9	3	3	2	81.02
K1	253.35	252.94	240.89	
K2	264.53	257.12	268.03	
K3	234.06	241.88	243.02	
k1	84.45	84.31	80.30	
k2	88.18	85.71	89.34	
k3	78.02	80.63	81.01	
R	10.16	5.08	9.05	

Table 4 Results of Variance Analysis on Particle Size

Source of Variance	Sum of Squares of Deviation	Degree of Freedom (Df)	Mean Square	F	P
A	46585.39	2	23,292.69	6.47	>0.05
B	38517.80	2	19,258.90	5.35	>0.05
C	16767.42	2	8383.71	2.33	>0.05
Error	7201.80	2	3600.90		

Table 5 Results of Variance Analysis on EE%

Source of Variance	Sum of Squares of Deviation	Degree of Freedom (Df)	Mean Square	F	P
A	158.41	2	79.20	24.20	<0.05
B	41.36	2	20.68	6.32	>0.05
C	151.78	2	75.89	23.19	<0.05
Error	6.55	2	3.72		

formulation was determined to be $A_2B_2C_2$, namely, BSA concentration of 22.4 mg/mL, DTX concentration of 5 mg/mL, and incubation time of 3 min.

Effects of Preparation Process on DTX-BSA-NPs Prepared by Thermal-Driven Self-Assembly/Microfluidic Technology

Currently, the key challenges in BSA NP preparation include controlling the particle size, enhancing the stability, and reducing batch-to-batch variations in industrial production.[28,29,56] Utilizing microfluidic technology for NP preparation offers precise control over the particle size, heightened stability, enhanced EE, and improved production consistency.[57–59] This utilization addresses crucial issues in the preparation process, thus ensuring product quality and uniformity. Therefore, a combination of heat-driven self-assembly and microfluidic technology was used to prepare DTX-BSA-NPs. The effects of flow rate and pump pressure on DTX-BSA-NPs were mainly investigated in this study, because the properties of nanoscale formulations prepared using microfluidic technology are influenced by both factors.[60–62]

Recent studies have shown that the properties of NPs prepared by microfluidic technology can be tuned by adjusting the volumetric flow rate ratio (FRR) between the lipid and water phase streams, and the total flow rate (TFR).[63–65] In the present study, the FRR was fixed at 1:2. Three different TFRs were set at 3, 6, and 12 mL/min. Specifically, the flow rates of the organic phase were set at 1, 2, and 4 mL/min, with corresponding water phase flow rates of 2, 4, and 8 mL/min. Figure 4A and C display the effects of flow rate on the particle size, EE, and DL of DTX-BSA-NPs. When the flow rates of the organic and water phases were set at 2 and 4 mL/min, respectively, the DTX-BSA-NPs showed a particle size of 113.37 nm, an EE of 86.51%, and a DL of 8.93%. The particle size of DTX-BSA-NPs was observed to reduce with increasing TFR, which was in accordance with previous research.[64]

Figure 4B and D show the influence of pump pressure on the properties of NPs. As the pressure increased, the particle size and EE of DTX-BSA-NPs decreased. The mean particle size was 121.47 nm, the EE was 86.25%, and the DL was 8.31%, indicating that DTX-BSA-NPs are more suitable to be prepared without applying pressure. Thus, the preparation process was optimized with an organic phase flow rate of 2 mL/min and an aqueous phase flow rate of 4 mL/min, without applying pump pressure.

Reproducibility Study

Three batches of optimized formulation were prepared to compare the batch-to-batch variations of NPs. As shown Figure 5A and B, the particle size, zeta potential, EE, and DL of the three batches of NPs showed a good reproducibility, with high EE and DL capacity. As shown in Figure 5C and D, the particle size, EE, and DL after

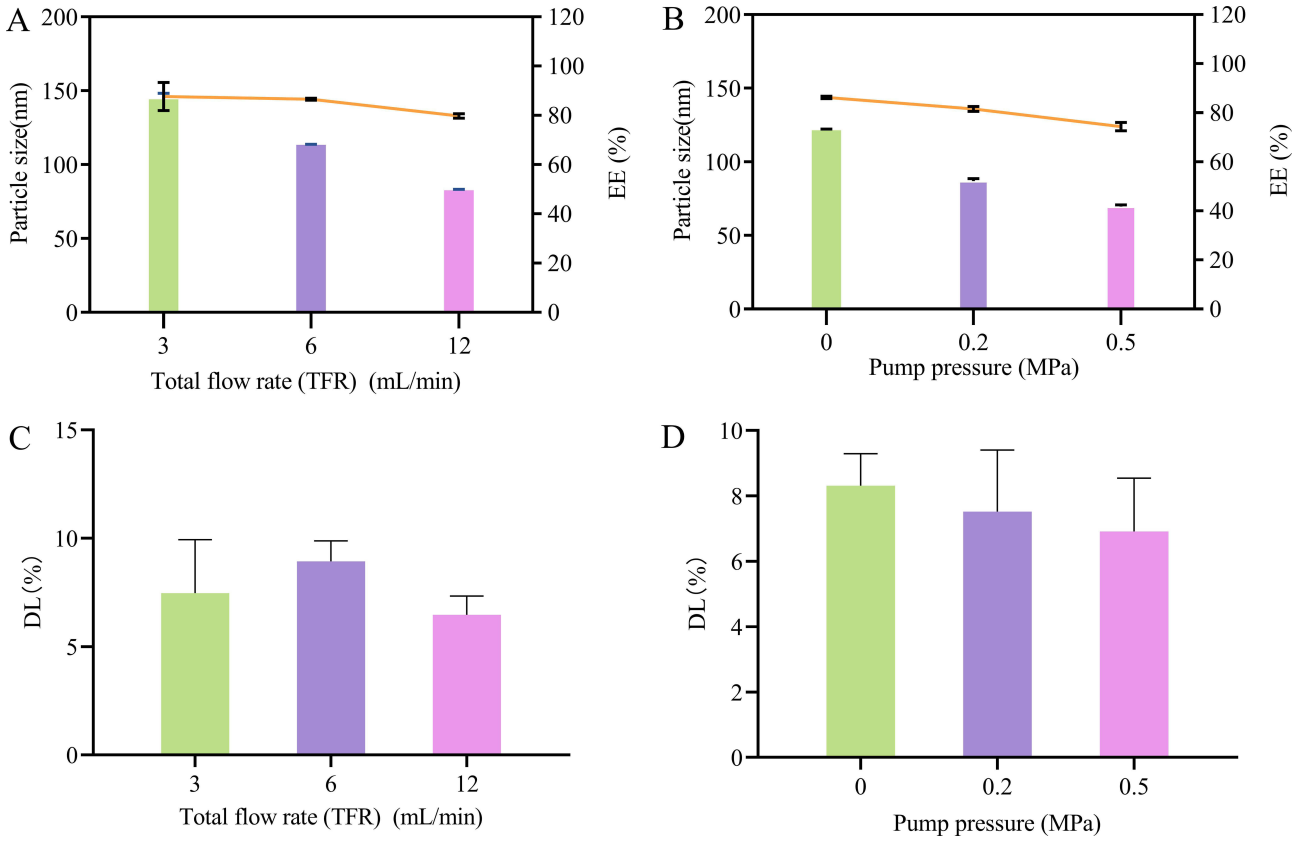

Figure 4 Effects of Preparation process on DTX-BSA-NPs. (**A** and **B**) show the effect of flow rate and pump pressure on particle size and EE, with color bars indicating particle size and a line chart displaying EE. (**C** and **D**) show the effect of flow rate and pump pressure on DL. All data are presented as mean±SD (n=3).

reconstitution of the three batches of freeze-dried NPs were identical when compared with one another, indicating the commendable reproducibility of the freeze-dried formulation. Meanwhile, the particle size, EE, and DL of NPs between pre- and post-freeze drying were compared. As shown in Figure 5E and F, the freeze drying had no effect on the particle size, EE, and DL. Before freeze drying, the average particle size of DTX-BSA-NPs was 118.30 nm, with a polydispersity index (PDI) of 0.251 (Figure 5G). After freeze drying, the average particle size was measured as 119.40 nm, with a PDI of 0.250 (Figure 5H). These findings demonstrated no significant changes in the particle size or distribution before and after freeze drying, suggesting that freeze drying did not significantly affect the particle size of DTX-BSA-NPs. Addressing batch-to-batch variability in the industrial production of BSA NPs is a complex challenge that encompasses various factors, from the physicochemical characteristics of the nanoparticles to the synthesis and processing parameters.[66,67] In this study, both BSA NPs and freeze-dried powders exhibit good reproducibility. The formulation composition and manufacturing process of DTX-BSA-NPs were successfully optimized by the thermal-driven self-assembly/microfluidic combination technology, providing an experimental foundation for future industrial-scale production.

Appearance and Morphology of NPs

As shown in Figure 6, the cake-like appearance and non-collapsed property of DTX-BSA-NP powders are indicative of successful freeze drying process. The morphology is essential for ensuring the stability of NPs and can facilitate the quick reconstitution of freeze-dried powders. Upon reconstitution with distilled water/or physiological saline, it transformed into a gelatinous solution that retained a lustrous blue.

The TEM images in Figure 7 showed that the DTX-BSA-NPs had well-dispersed and spherical shapes with uniform particle size.

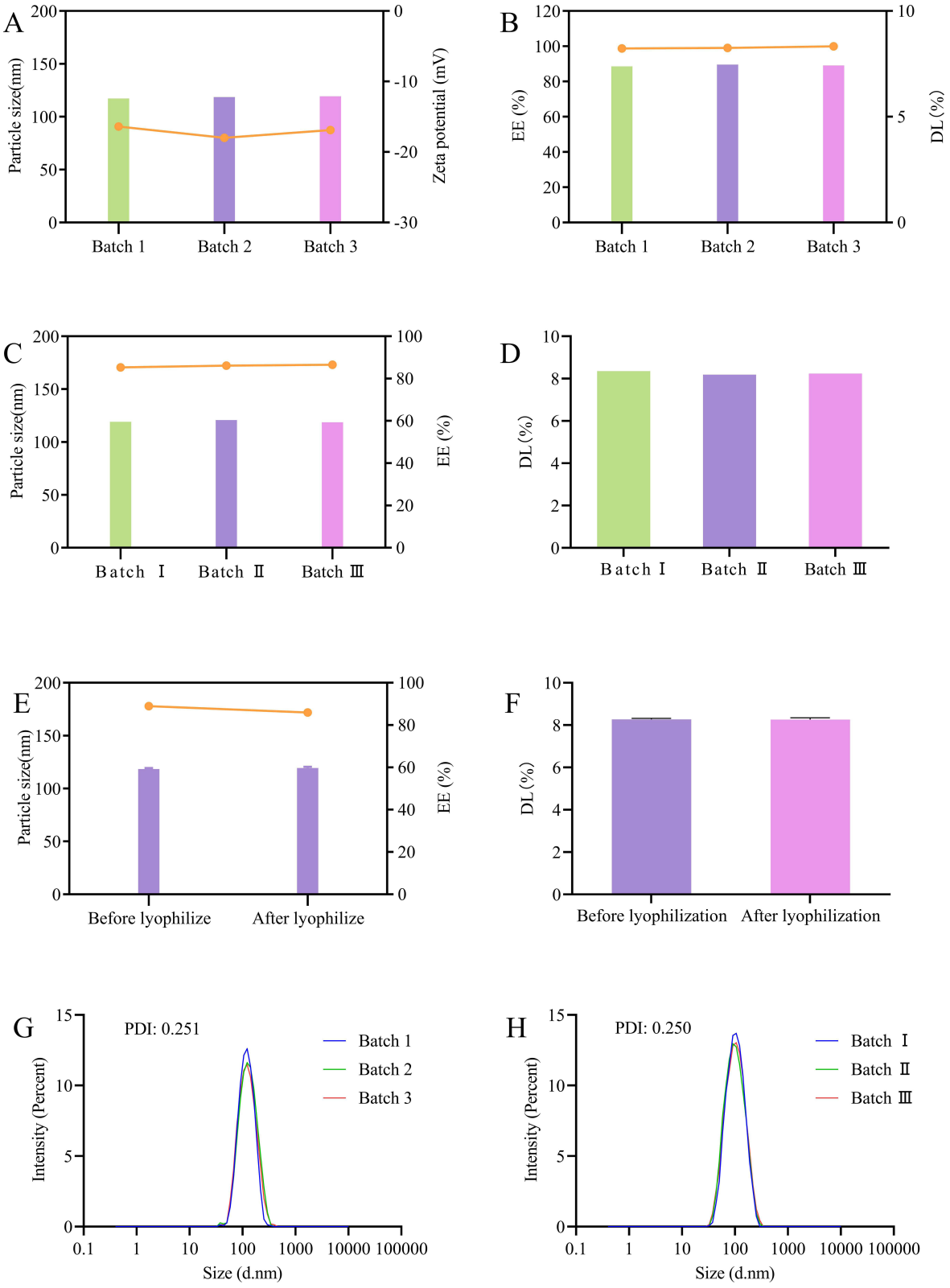

Figure 5 Batch-to-batch reproducibility and freeze drying stability of DTX-BSA-NPs. (**A**) the particle size and zeta potential of three different batches, with color bars indicating particle size and a line chart displaying zeta potential. (**B**) the EE and DL of three different batches, with color bars indicating EE and a line chart displaying DL. (**C**) the consistency in particle size and EE of freeze-dried NPs upon reconstitution, with color bars indicating particle size and a line chart displaying EE. (**D**) the consistency in DL of freeze-dried NPs upon reconstitution. (**E**) the particle size and EE before and after freeze drying, with color bars indicating particle size and a line chart displaying EE. (**F**) the DL of freeze-dried NPs before and after freeze drying. (**G** and **H**) the PDI of DTX-BSA-NPs before and after freeze drying. All data are presented as mean±SD (n=3).

Figure 6 Appearance of freeze-dried powder and reconstituted suspension of DTX-BSA-NPs. (Left: freeze-dried powder; Right: reconstituted suspension).

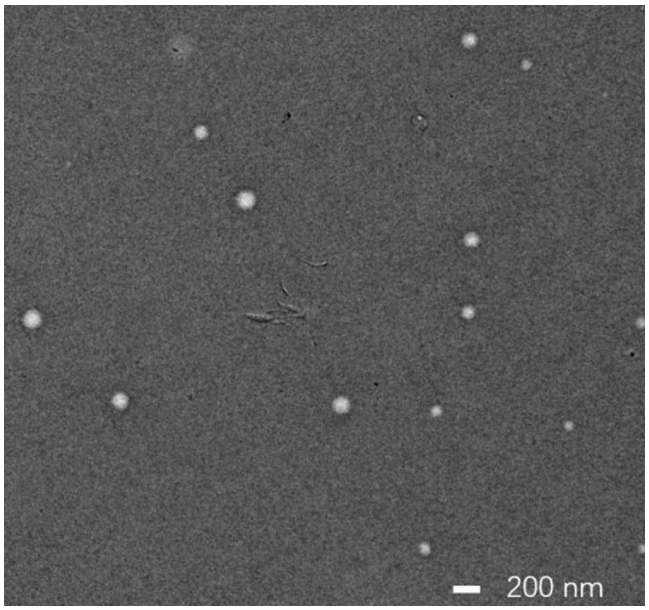

Figure 7 TEM images of DTX-BSA-NPs. Scale bar = 200 nm.

DSC

DSC is a technique that monitors the physical properties of a substance by employing a controlled temperature program.[68,69] The DSC spectra of DTX; BSA; physical mixture of DTX, BSA, and sodium gluconate; and DTX-BSA-NPs are illustrated in Figure 8. The endothermic peak of DTX around 170°C was found, which is consistent with the reported melting point range of DTX in literature.[70] In addition, an exothermic event around 220°C was observed, which may be related to the decomposition process.[71] The endothermic peak at 224°C represents thermal degradation of BSA.[72] The characteristic peaks of DTX and BSA were shown in the spectra of the mixture of DTX, BSA, and sodium gluconate. However, for DTX-BSA-NPs, the characteristic peaks of DTX and BSA disappeared, indicating that the physical properties of DTX were changed in the DTX-BSA NP matrix.

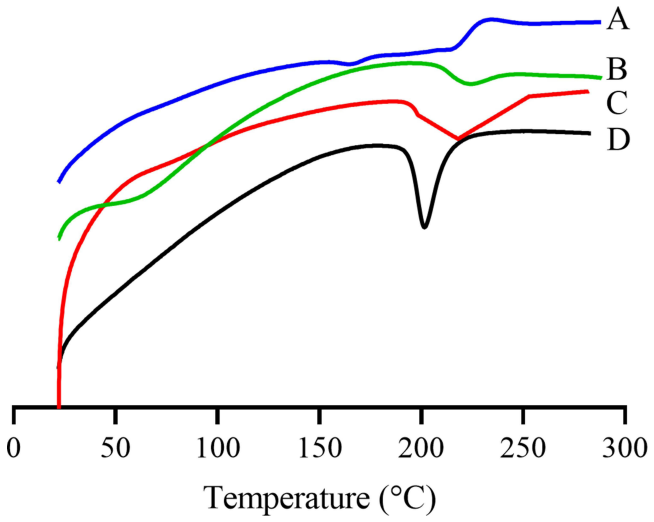

Figure 8 DSC spectra of (**A**) DTX, (**B**) BSA, (**C**) physical mixture of DTX, BSA and sodium gluconate, and (**D**) DTX-BSA-NPs.

FTIR

FTIR is an analytical technique employed to determine the existence of functional groups and the extent of crosslinking, and it can be used to detect the interactions between drug and NPs through the change in characteristic peak of the group.[73,74]

The FTIR results of pure drug; BSA; physical mixture of DTX, BSA, and sodium gluconate; and DTX-BSA-NPs are presented in Figure 9. The characteristic adsorption peaks of DTX at 3533.41 and 3463.7cm^{-1} can be attributed to N-H stretching and O-H stretching, respectively. The peaks at 1722.34 and 1706.92 cm^{-1} may be ascribed to C=O stretching vibration.[73] The bands at 1164.9 and 1247.9 cm^{-1} can be attributed to C-O stretching of ester.[75] The spectrum also showed bands at 1492.8 and 1452.3 cm^{-1}, indicating C=C aromatic ring.[71] The absorption peak of BSA at 1647.1 cm^{-1} belongs to C=O stretching. The peak at 1521.7 cm^{-1} is related to C-N stretching and N-H bending vibrations.[76,77] The characteristic adsorption peaks of DTX and BSA were shown in the spectra of the mixture of DTX, BSA, and sodium gluconate. However, the absorption peaks of DTX, including the bands at 1492.8, 1452.3, 1164.9, and 1247.9 cm^{-1}, were remarkably diminished in the DTX-BSA-NPs. This finding suggested that some interactions may have occurred between DTX and the carriers during the preparation of DTX-BSA-NPs.

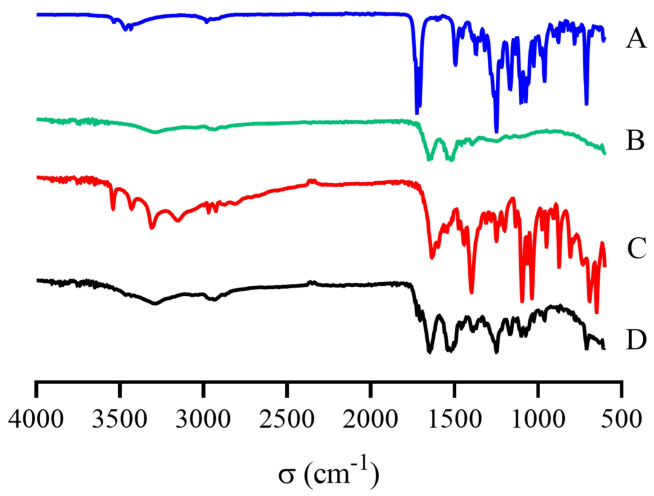

Figure 9 FT-IR spectra of (**A**) DTX, (**B**) BSA, (**C**) physical mixture of DTX, BSA and sodium gluconate, and (**D**) DTX-BSA-NPs.

In-Vitro Release

The cumulative release curves of DTX-BSA-NPs and DTX are shown in Figure 10. The results demonstrated that the release rate of DTX reached over 80% at 36 h, whereas DTX-BSA-NPs exhibited a cumulative release of 2.76% only at 0.5 h, without any initial burst release. Furthermore, the cumulative release rate of DTX-BSA-NPs approached 70% at 96 h, indicating a significant sustained-release effect. The sustained release of DTX-BSA-NPs followed a distinct diffusion pattern of drug molecules from the hydrophobic core within the albumin nanosystem.[76,78,79] The release properties of BSA NPs may be attributed to the stiffening of the polymeric network during crosslinking.[80] The BSA shell formed on the surface of drug particle can provide a steric stabilization effect, for retarding the release rate and reducing side effects of the drug.[81]

Stability Study

Conducting stability influencing factor studies and accelerated stability testing is essential to investigate the inherent stability of a pharmaceutical product or formulation; understand the factors affecting its stability, potential degradation pathways, and degradation products; and provide scientific evidence for formulation production processes, packaging, and storage conditions.[82,83]

Figure 11 shows the results of stability test under stress conditions. DTX showed slight precipitation after 10 days of exposure to strong light (4500 ± 500 Lx) or high temperature (60°C), whereas the appearance of the self-prepared DTX-BSA-NPs remained unchanged and showed good redispersibility. Figure 11A and B show the influence of strong light on pH and drug content. The pH of DTX decreased from 6.0 to 5.4 after 15 days of strong illumination, whereas that of the self-prepared freeze-dried DTX-BSA-NPs decreased by 0.3 only. After 30 days of light exposure, the drug content of DTX decreased rapidly to 23.37%, whereas the self-prepared freeze-dried DTX-BSA-NPs showed a drug content of 63.81%. Figure 11C and D show the influence of high temperature on pH and drug content. The pH of DTX decreased from 6.0 to 4.4 after 15 days under high temperature, whereas that of the self-prepared freeze-dried DTX-BSA-NPs decreased by 0.5 only. After 30 days of exposure to high temperature, the drug content of DTX decreased rapidly to 39.19%, whereas the self-prepared freeze-dried DTX-BSA-NPs showed a drug content of 69.89%. High humidity (92.5% RH) had a significant influence on the appearance of DTX and the self-prepared freeze-dried DTX-BSA-NPs. After being exposed to high temperature for 10 days, DTX displayed a slight presence of precipitation, whereas the DTX-BSA-NPs exhibited a tendency towards agglomeration and a noticeable decline in redispersibility after 15 days of storage. Figure 11E and F show the influence of high humidity on pH and drug content. The pH of DTX decreased from 6.0 to 5.3 after 30 days under high humidity, and that of the self-prepared freeze-dried DTX-BSA-NPs decreased from 7.8 to 7.1. After being exposed to high humidity for 30 days, the drug content of DTX decreased rapidly to 29.18%, whereas the self-prepared freeze-dried DTX-BSA-NPs showed a drug content of 59.86%. The results showed that the degradation

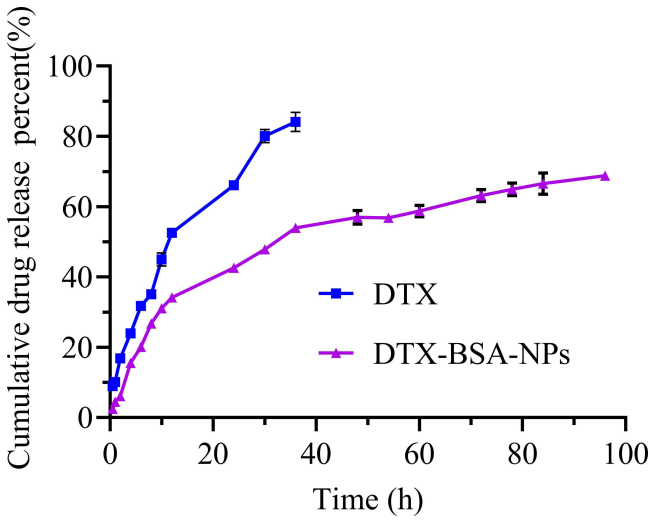

Figure 10 In-vitro release profiles of DTX-BSA-NPs and DTX. All data are presented as mean±SD (n=3).

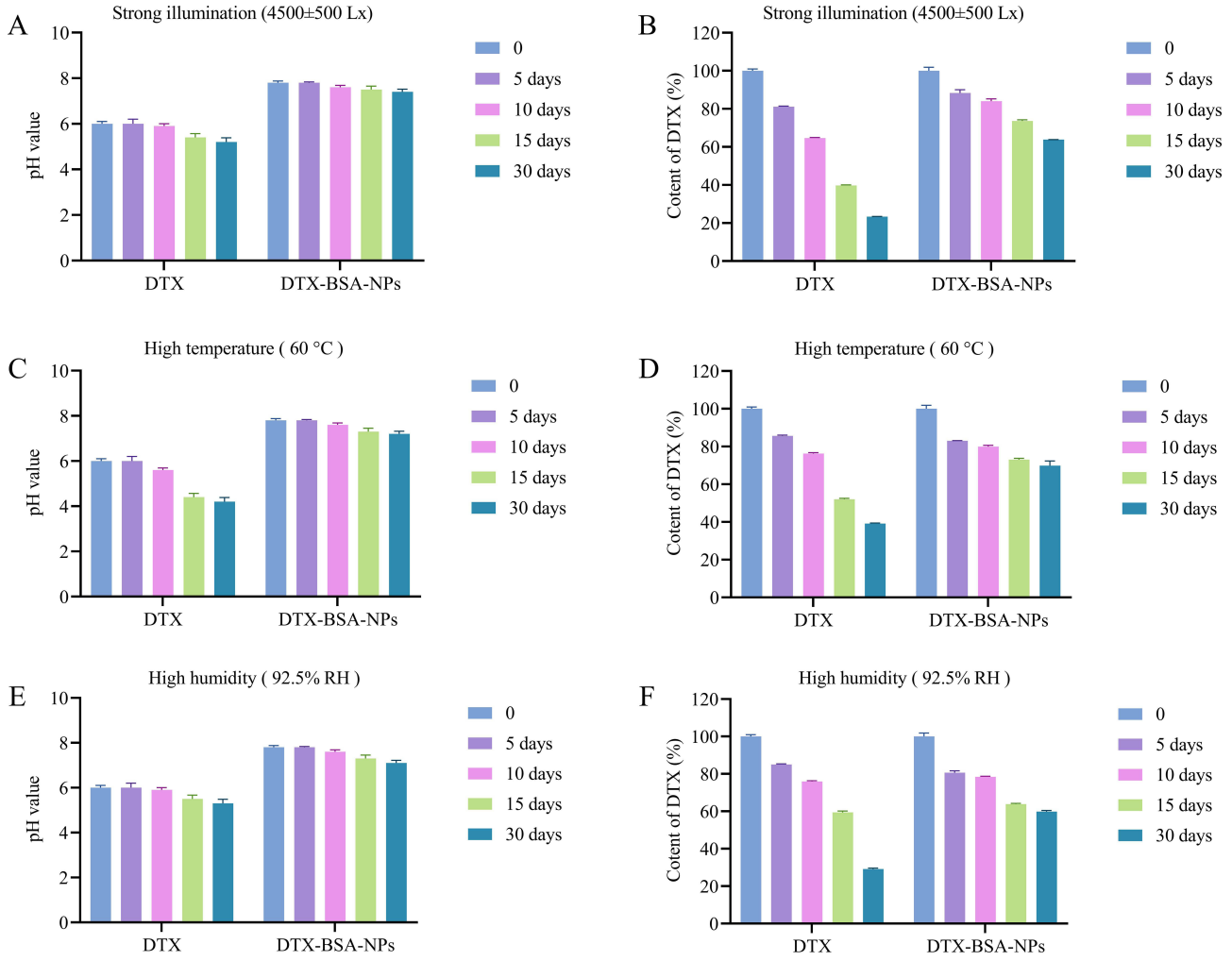

Figure 11 Stress test of commercial product (DTX) and DTX-BSA-NP powders. (**A** and **B**) illustrate the influence of strong light (4500±500 Lx) on pH value and content of DTX. (**C** and **D**) present the impact of high temperature (60±2°C) on pH value and content of DTX. (**E** and **F**) demonstrate the influence of high humidity (92.5±5% RH) on pH value and content of DTX. All data are presented as mean±SD (n=3).

rate of the self-prepared freeze-dried DTX-BSA-NPs was much slower than that of DTX. A possible reason was that the encapsulation of DTX into BSA prevented leakage during storage, and the sample was in the form of freeze-dried powder, which facilitated slow degradation under conditions of strong light, high temperature, and high humidity.

Figure 12 shows the results of accelerated stability test. Figure 12A and B show the pH and drug content changes in DTX and DTX-BSA-NPs at 25°C. When the preparations were stored for 3 months, a small amount of precipitation was found in DTX, with a drop in pH to 5.4, and the drug content was 79.89% ± 0.54%. On the contrary, no significant changes were found in the appearance of the freeze-dried DTX-BSA-NPs. The redispersibility was good, the pH decreased by 0.3 only, and the drug content reduced to 85.74% only. Figure 12C and D show the pH and drug content changes in DTX and DTX-BSA-NPs at 40°C. When DTX was stored for 3 months, a small amount of precipitation was observed, the pH decreased to 5.3, and the drug content was 65.65%. However, the freeze-dried DTX-BSA-NPs showed no significant changes in appearance, the redispersibility was good, the pH decreased by 0.6, and the drug content reduced to 66.76%. These results showed that the freeze-dried powder showed higher stability than DTX, but it still needed to be kept at low temperature.

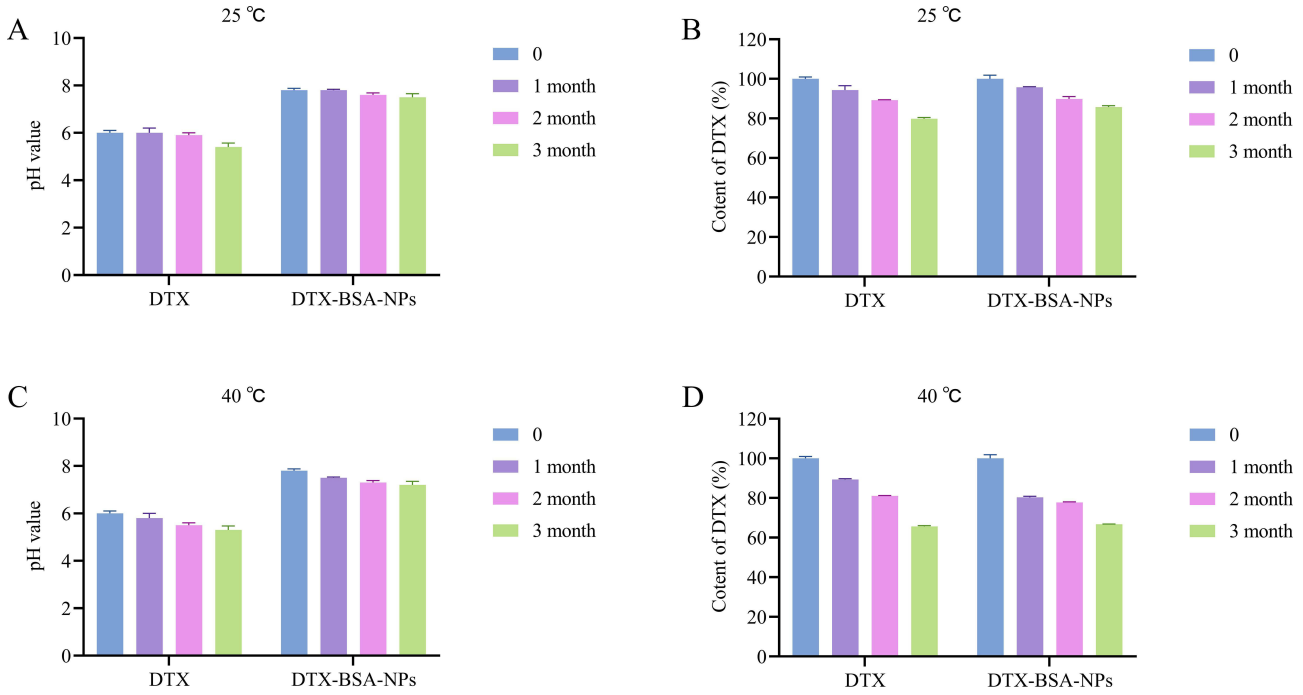

Figure 12 Accelerated test of DTX and DTX-BSA-NPs. (**A** and **B**) illustrate the changes in pH value and DTX content under storage at 25°C. (**C** and **D**) present the variation of pH value and DTX content at 40°C. All data are presented as mean±SD (n=3).

Pharmacokinetic Study

The in-vivo bioavailability of poorly soluble drugs can be effectively enhanced by encapsulation in BSA NPs.[84–86] Figures 13 and 14 demonstrate the plasma concentration–time curves and pharmacokinetic parameters of DTX and DTX-BSA-NPs after intravenous injection. As illustrated in Figure 13, both formulations exhibited a rapid increase in the concentration of DTX post-administration, reflecting quick absorption. After attaining peak levels, the concentration of DTX in both formulations diminished progressively, signifying the drug's distribution and subsequent elimination from the body. The DTX-BSA-NPs showed a more gradual decrease in concentration than the DTX, indicating its slower release rate, which potentially leads to a longer duration of action. Over a 24 h period, the DTX-BSA-NPs maintained a higher concentration than the DTX. This sustained release profile aligns with the results observed from in-vitro release studies. As shown in Figure 14, no significant difference was found in the C_{max} and $T_{1/2\alpha}$ values between DTX and DTX-

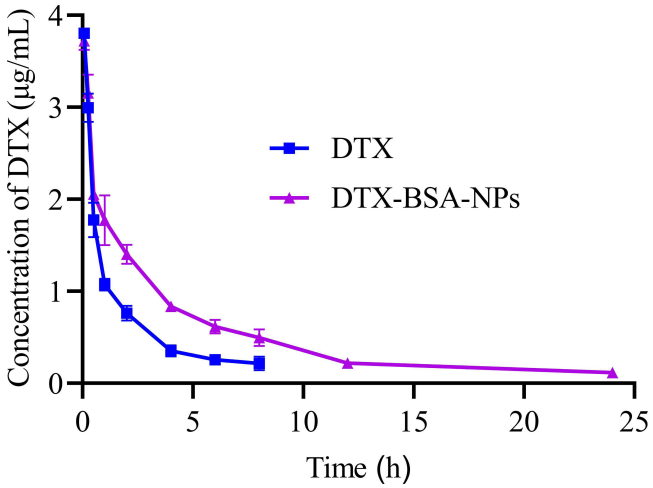

Figure 13 Pharmacokinetic profiles of DTX concentration over time following iv injection of DTX and DTX-BSA-NPs to SD rats (n=5).

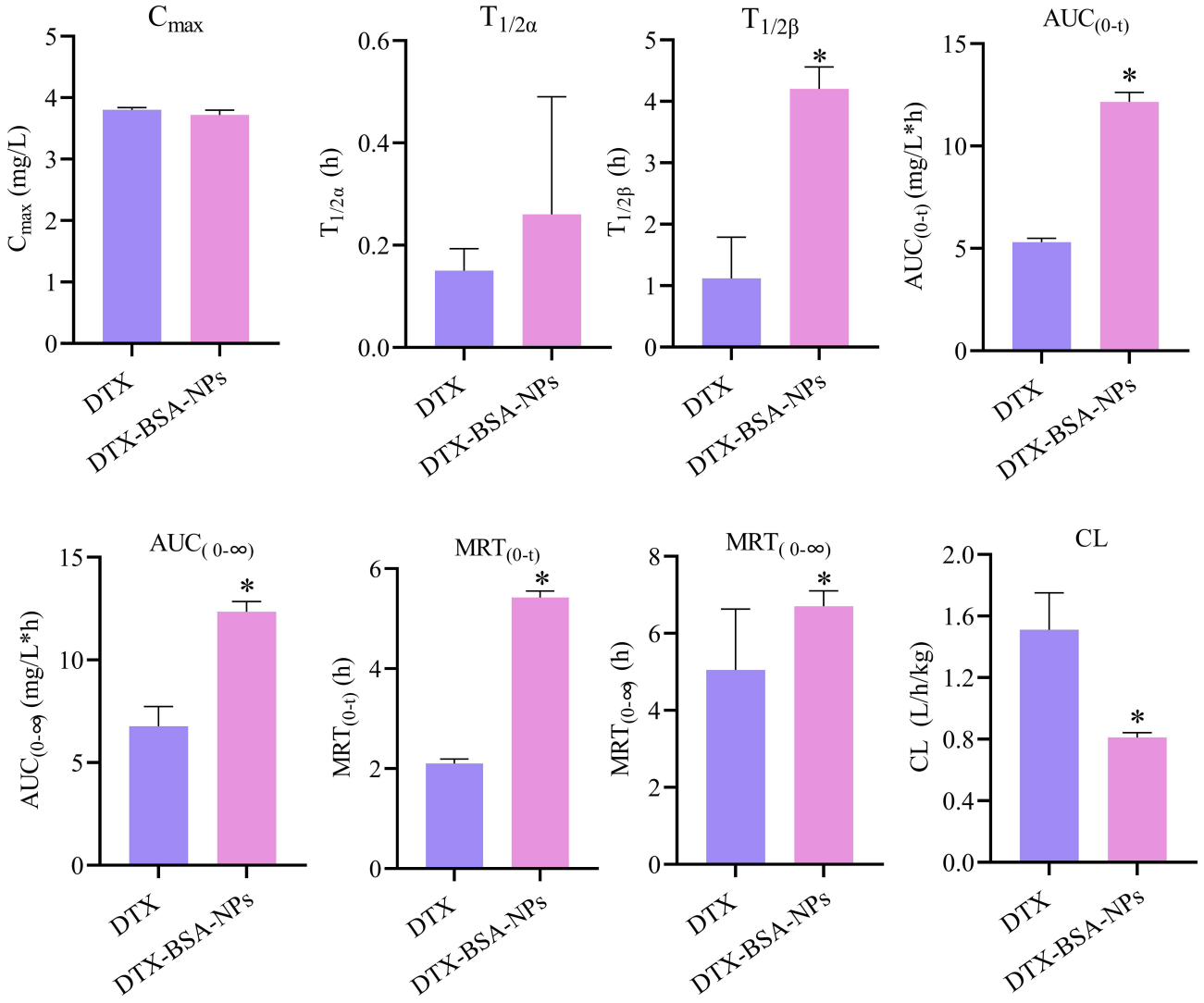

Figure 14 Pharmacokinetic parameters of DTX and DTX-BSA-NPs in SD rats (n=5), *p<0.05, significant difference compared with DTX group.

BSA-NPs. However, the drug was rapidly cleared from the bloodstream for DTX, resulting in a $T_{1/2\beta}$ of 1.12 h only. By contrast, the DTX-BSA-NPs exhibited an extended $T_{1/2\beta}$ of 4.20 h compared with DTX ($p < 0.05$). Even after 24 h of injection, the drug concentration remained detectable in the serum. The $AUC_{(0\text{-}t)}$ of the DTX-BSA-NP group increased by 2.29-fold compared with that of the DTX group (12.16 ± 0.46 mg/L*h vs 5.31 ± 0.18 mg/L*h, $p < 0.05$), indicating a higher relative bioavailability (around 229 ±3%) for BSA NPs than for the DTX solution.[12,87] The $MRT_{(0\text{-}t)}$ of DTX-BSA-NPs was 2.58-fold higher than that of DTX, suggesting that the BSA-NPs extended the average residence time of DTX. Compared with the DTX group, the DTX-BSA-NP group showed a decrease in CL from 1.51 L/h/kg to 0.81 L/h/kg ($p < 0.05$). The increase in AUC and MRT and the reduction in CL indicate that the DTX-BSA-NPs can circulate in the blood for a longer duration. This phenomenon might be caused by the sustained release of DTX and decreased tissue distribution of DTX-BSA-NPs.[81,88] It was also found that the hydrophobic amino acid residues, such as alanine and isoleucine, found in BSA are likely to enhance the binding of drug molecule through hydrophobic interactions, and further cause the enhanced bioavailability of DTX.[89,90]

Conclusion

The commercial DTX formulated with polysorbate 80 and ethanol (50:50, v/v), causes allergic reactions and serious side effects. In this study, surfactant-free DTX-BSA-NPs were designed by a novel thermal-driven self-assembly/microfluidic

combination technology using BSA as a carrier with good biocompatibility, non-toxicity and non-immunogenicity. The formulation composition and preparation process were optimized by a single-factor analysis and an orthogonal test. The optimal NPs exhibited an appropriate particle size with high EE and DL. The freeze-dried DTX-BSA-NP powders showed no significant changes compared with NP suspensions in particle size, EE, and DL. DTX-BSA-NPs showed an obvious sustained release pattern with some interactions between the drug and excipients. The freeze-dried DTX-BSA-NPs exhibited a higher stability than DTX under different storage conditions. In addition, DTX-BSA-NPs also possessed the ability to prolong the circulation within the body, thereby further enhancing the bioavailability of DTX. This research could provide theoretical and experimental foundation for the industrialization and production of DTX-BSA-NPs.

Acknowledgments

This work was supported by the projects funded by the Priority Academic Program Development (PAPD) of Jiangsu Higher Education Institutions and the Jiangsu Province Engineering Research Center of Precision Diagnostics and Therapeutics Development, Soochow University (CN). This work was also funded by the Zhejiang Provincial Education Department research projects (Y202352274).

Disclosure

The authors report no conflicts of interest in this work.

References

1. Jurczyk M, Kasperczyk J, Wrzesniok D, et al. Nanoparticles loaded with docetaxel and resveratrol as an advanced tool for cancer therapy. *Biomedicines*. 2022;10(5):1187. doi:10.3390/biomedicines10051187
2. Al-Nemrawi NK, Altawabeyeh RM, Darweesh RS. Preparation and characterization of docetaxel-PLGA nanoparticles coated with folic acid-chitosan conjugate for cancer treatment. *J Pharm Sci*. 2022;111(2):485–494. doi:10.1016/j.xphs.2021.10.034
3. Zhu XJ, Yu ZJ, Feng LB, et al. Chitosan-based nanoparticle co-delivery of docetaxel and curcumin ameliorates anti-tumor chemoimmunotherapy in lung cancer. *Carbohydr Polym*. 2021;268:118237. doi:10.1016/j.carbpol.2021.118237
4. Emami J, Kazemi M, Hasanzadeh F, et al. Novel pH-triggered biocompatible polymeric micelles based on heparin-alpha-tocopherol conjugate for intracellular delivery of docetaxel in breast cancer. *Pharm Dev Technol*. 2020;25(4):492–509. doi:10.1080/10837450.2019.1711395
5. Gu ZL, Wang QJ, Shi YB, et al. Nanotechnology-mediated immunochemotherapy combined with docetaxel and PD-L1 antibody increase therapeutic effects and decrease systemic toxicity. *J Control Release*. 2018;286:369–380. doi:10.1016/j.jconrel.2018.08.011
6. Vakili-Ghartavol R, Mehrabian A, Mirzavi F, et al. Docetaxel in combination with metformin enhances antitumour efficacy in metastatic breast carcinoma models: a promising cancer targeting based on PEGylated liposomes. *J Pharm Pharmacol*. 2022;74(9):1307–1319. doi:10.1093/jpp/rgac048
7. Jain S, Deore SV, Ghadi R, et al. Tumor microenvironment responsive VEGF-antibody functionalized pH sensitive liposomes of docetaxel for augmented breast cancer therapy. *Mater Sci Eng C Mater Biol Appl*. 2021;121:111832. doi:10.1016/j.msec.2020.111832
8. Gu ZL, Da Silva CG, Hao Y, et al. Effective combination of liposome-targeted chemotherapy and PD-L1 blockade of murine colon cancer. *J Control Release*. 2023;353:490–506. doi:10.1016/j.jconrel.2022.11.049
9. Tran P, Nguyen TN, Lee Y, et al. Docetaxel-loaded PLGA nanoparticles to increase pharmacological sensitivity in MDA-MB-231 and MCF-7 breast cancer cells. *Korean J Physiol Pharmacol*. 2021;25(5):479–488. doi:10.4196/kjpp.2021.25.5.479
10. Ren LL, Nie JF, Wei J, et al. RGD-targeted reDTX responsive nano micelle: co-loading docetaxel and indocyanine green to treat the tumor. *Drug Deliv*. 2021;28(1):2024–2032. doi:10.1080/10717544.2021.1977425
11. Tao J, Diao L, Chen FC, et al. pH-sensitive nanoparticles codelivering docetaxel and dihydroartemisinin effectively treat breast cancer by enhancing reactive oxidative species-mediated mitochondrial apoptosis. *Mol Pharm*. 2021;18(1):74–86. doi:10.1021/acs.molpharmaceut.0c00432
12. Wang WP, Lei YY, Sui H, et al. Fabrication and evaluation of nanoparticle-assembled BSA microparticles for enhanced liver delivery of glycyrrhetinic acid. *Artif Cells Nanomed Biotechnol*. 2017;45(4):740–747. doi:10.1080/21691401.2016.1193024
13. Desale JP, Swami RJ, Kushwah V, et al. Chemosensitizer and docetaxel-loaded albumin nanoparticle: overcoming drug resistance and improving therapeutic efficacy. *Nanomedicine*. 2018;13(21):2759–2776. doi:10.2217/nnm-2018-0206
14. Huang YK, Hu L, Huang S, et al. Curcumin-loaded galactosylated BSA nanoparticles as targeted drug delivery carriers inhibit hepatocellular carcinoma cell proliferation and migration. *Int J Nanomed*. 2018;13:8309–8323. doi:10.2147/IJN.S184379
15. Sleep D. Albumin and its application in drug delivery. *Expert Opin Drug Deliv*. 2015;12(5):793–812. doi:10.1517/17425247.2015.993313
16. Wang YF, Chen S, Yang X, et al. Preparation optimization of bovine serum albumin nanoparticles and its application for siRNA delivery. *Drug Des Devel Ther*. 2021;15:1531–1547. doi:10.2147/DDDT.S299479
17. Desai NP, Soon-Shiong P Therapy for breast cancer based on hormone receptor status with nanoparticles comprising taxane. United States Patent, Patent No: US 8999 396 B2. 2015 Apr 7.
18. Lluch A, Alvarez I, Munoz M, et al. Treatment innovations for metastatic breast cancer: nanoparticle ´ albumin-bound (NAB) technology targeted to tumors. *Crit Rev Oncol Hematol*. 2014;89(1):62–72. doi:10.1016/j.critrevonc.2013.08.001
19. Miele E, Spinelli GP, Miele E, et al. Albumin-bound formulation of paclitaxel (Abraxane ABI-007) in the treatment of breast cancer. *Int J Nanomed*. 2009;4:99–105. doi:10.2147/ijn.s3061
20. Sristi, Fatima M, Sheikh A, et al. Recent advancement on albumin nanoparticles in treating lung carcinoma. *J Drug Target*. 2023;31(5):486–499. doi:10.1080/1061186X.2023.2205609

21. Yuan DM, Lv YL, Yao YW, et al. Efficacy and safety of Abraxane in treatment of progressive and recurrent non-small cell lung cancer patients: a retrospective clinical study. *Thorac Cancer*. 2012;3(4):341–347. doi:10.1111/j.1759-7714.2012.00113.x
22. Herper M. Celgene's Abraxane extends life by 1.8 months in advanced pancreatic cancer. *Forbes com*. 2013;23:9.
23. Loureiro A, Azoia NG, Gomes AC, et al. Albumin-based nanodevices as drug carriers. *Curr Pharm Des*. 2016;22(10):1371–1390. doi:10.2174/1381612822666160125114900
24. Rostamabadi H, Falsafi SR, Jafari SM. Starch-based nanocarriers as cutting-edge natural cargos for nutraceutical delivery. *Trends Food Sci Technol*. 2019;88:397–415. doi:10.1016/j.tifs.2019.04.004
25. Arpagaus C, Collenberg A, Rutti D, et al. Nano spray drying for encapsulation of pharmaceuticals. *Int J Pharm*. 2018;546(1–2):194–214. doi:10.1016/j.ijpharm.2018.05.037
26. Strojewski D, Krupa A. Spray drying and nano spray drying as manufacturing methods of drug-loaded polymeric particles. *Polim Med*. 2022;52(2):101–111. doi:10.17219/pim/152230
27. Fu Q, Sun J, Zhang WP, et al. Nanoparticle albumin-bound (NAB) technology is a promising method for anti-cancer drug delivery. *Recent Pat Anticancer Drug Discov*. 2009;4(3):262–272. doi:10.2174/157489209789206869
28. Elzoghby AO, Samy WM, Elgindy NA. Albumin-based nanoparticles as potential controlled release drug delivery systems. *J Control Release*. 2012;157(2):168–182. doi:10.1016/j.jconrel.2011.07.031
29. Solanki R, Rostamabadi H, Patel S, et al. Anticancer nano-delivery systems based on bovine serum albumin nanoparticles: a critical review. *Int J Biol Macromol*. 2021;193:528–540. doi:10.1016/j.ijbiomac.2021.10.040
30. Hassanin IA, Elzoghby AO. Self-assembled non-covalent protein-drug nanoparticles: an emerging delivery platform for anti-cancer drugs. *Expert Opin Drug Deliv*. 2020;17(10):1437–1458. doi:10.1080/17425247.2020.1813713
31. Crisante F, Francolini I, Bellusci M, et al. Antibiotic delivery polyurethanes containing albumin and polyallylamine nanoparticles. *Eur J Pharm Sci*. 2009;36(4–5):555–564. doi:10.1016/j.ejps.2008.12.006
32. Langer K, Anhorn MG, Steinhauser I, et al. Human serum albumin (HSA) nanoparticles: reproducibility of preparation process and kinetics of enzymatic degradation. *Int J Pharm*. 2008;347(1–2):109–117. doi:10.1016/j.ijpharm.2007.06.028
33. Yedomon B, Fessi H, Charcosset C. Preparation of Bovine Serum Albumin (BSA) nanoparticles by desolvation using a membrane contactor: a new tool for large scale production. *Eur J Pharm Biopharm*. 2013;85:398–405. doi:10.1016/j.ejpb.2013.06.014
34. Manz A, Graber N, Widmer HM. Miniaturized total chemical analysis systems: a novel concept for chemical sensing. *Sensor Actuat B-Chem*. 1990;1(1–6):244–248. doi:10.1016/0925-4005(90)80209-I
35. Kopp MRG, Linsenmeier M, Hettich B, et al. Microfluidic shrinking droplet concentrator for analyte detection and phase separation of protein solutions. *Anal Chem*. 2020;92(8):5803–5812. doi:10.1021/acs.analchem.9b05329
36. Chung MT, Kurabayashi K, Cai D. Single-cell RT-LAMP mRNA detection by integrated droplet sorting and merging. *Lab Chip*. 2019;19(14):2425–2434. doi:10.1039/c9lc00161a
37. Utharala R, Tseng QZ, Furlong EEM, et al. A versatile, low-cost, multiway microfluidic sorter for droplets, cells, and embryos. *Anal Chem*. 2018;90(10):5982–5988. doi:10.1021/acs.analchem.7b04689
38. Shang L, Cheng Y, Zhao YJ. Emerging droplet microfluidics. *Chem Rev*. 2017;117(12):7964–8040. doi:10.1021/acs.chemrev.6b00848
39. Liu DF, Zhang HB, Cito S, et al. Core/shell nanocomposites produced by superfast sequential microfluidic nanoprecipitation. *Nano Lett*. 2017;17(2):606–614. doi:10.1021/acs.nanolett.6b03251
40. Yang XL, Ju XJ, Mu XT, et al. Core-shell chitosan microcapsules for programmed sequential drug release. *ACS Appl Mater Interfaces*. 2016;8(16):10524–10534. doi:10.1021/acsami.6b01277
41. Maeki M, Ito S, Takeda R, et al. Room-temperature crystallography using a microfluidic protein crystal array device and its application to protein-ligand complex structure analysis. *Chem Sci*. 2020;11(34):9072–9087. doi:10.1039/d0sc02117b
42. Yang YY, Noviana E, Nguyen MP, et al. Paper-based microfluidic devices: emerging themes and applications. *Anal Chem*. 2017;89(1):71–91. doi:10.1021/acs.analchem.6b04581
43. Maeki M, Takeda R, Ishida A, et al. Real-time measurement of protein crystal growth rates within the microfluidic device to understand the microspace effect. *ACS Omega*. 2020;5(28):17199–17206. doi:10.1021/acsomega.0c01285
44. Song YL, Lin BQ, Tian T, et al. Recent progress in microfluidics-based biosensing. *Anal Chem*. 2019;91(1):388–404. doi:10.1021/acs.analchem.8b05007
45. Maeda H. Albumin-based drug delivery system targeting mannose receptors and its application to medical treatments. *Yakugaku Zasshi*. 2023;143(11):923–930. doi:10.1248/yakushi.23-00118
46. Meng R, Zhu HM, Deng PY, et al. Research progress on albumin-based hydrogels: properties, preparation methods, types and its application for antitumor-drug delivery and tissue engineering. *Front Bioeng Biotechnol*. 2023;11:1137145. doi:10.3389/fbioe.2023.1137145
47. Li F, Yeh S, Shi Q, et al. A novel thermal-driven self-assembly method to prepare albumin nanoparticles: formation kinetics, degradation behavior and formation mechanism. *AAPS Pharm Sci Tech*. 2022;23(7):250. doi:10.1208/s12249-022-02407-5
48. Qu N, Sun YT, Li YJ, et al. Docetaxel-loaded human serum albumin (HSA) nanoparticles: synthesis, characterization, and evaluation. *Biomed Eng Online*. 2019;18(1):11. doi:10.1186/s12938-019-0624-7
49. Asghar S, Salmani JMM, Hassan W, et al. A facile approach for crosslinker free nano self assembly of protein for anti-tumor drug delivery: factors' optimization, characterization and in vitro evaluation. *Eur J Pharm Sci*. 2014;63:53–62. doi:10.1016/j.ejps.2014.06.022
50. Rahimnejad M, Bakeri G. Investigation and modeling effective parameters influencing the size of BSA protein nanoparticles as colloidal carrier. *Colloids Surf A*. 2012;412:96–100. doi:10.1016/j.colsurfa.2012.07.022
51. Holm NK, Jespersen SK, Thomassen LV, et al. Aggregation and fibrillation of bovine serum albumin. *Biochim Biophys Acta*. 2007;1774(9):1128–1138. doi:10.1016/j.bbapap.2007.06.008
52. Rohanizadeh R, Kokabi N. Heat denatured/aggregated albumin-based biomaterial: effects of preparation parameters on biodegradability and mechanical properties. *J Mater Sci Mater Med*. 2009;20(12):2413–2418. doi:10.1007/s10856-009-3819-9
53. Honda C, Kamizono H, Samejima T, et al. Studies on thermal aggregation of bovine serum albumin as a drug carrier. *Chem Pharm Bull*. 2000;48(4):464–466. doi:10.1248/cpb.48.464
54. Ebel C, Eisenberg H, Ghirlando R. Probing protein-sugar interactions. *Biophys J*. 2000;78:385–393.

55. Taha M, Lee MJ. Interactions of TRIS [tris(hydroxymethyl)aminomethane] and related buffers with peptide backbone: thermodynamic characterization. *Phys Chem Chem Phys*. 2010;12(39):12840–12850. doi:10.1039/c0cp00253d
56. Shin JY, Cole BD, Seyedmohammad M, et al. Protein nanocarriers capable of encapsulating both hydrophobic and hydrophilic drugs. *Methods Mol Biol*. 2024;2720:143–150. doi:10.1007/978-1-0716-3469-1_10
57. Agha A, Waheed W, Stiharu I, et al. A review on microfluidic-assisted nanoparticle synthesis, and their applications using multiscale simulation methods. *Discov Nano*. 2023;18(1):18. doi:10.1186/s11671-023-03792-x
58. Yao FQ, Zhu PP, Chen JJ, et al. Synthesis of nanoparticles via microfluidic devices and integrated applications. *Mikrochim Acta*. 2023;190(7):256. doi:10.1007/s00604-023-05838-4
59. Fabozzi A, Sala FD, Di Gennaro M, et al. Design of functional nanoparticles by microfluidic platforms as advanced drug delivery systems for cancer therapy. *Lab Chip*. 2023;23(5):1389–1409. doi:10.1039/d2lc00933a
60. Zhang H, Yang J, Sun R, et al. Microfluidics for nano-drug delivery systems: from fundamentals to industrialization. *Acta Pharm Sin B*. 2023;13(8):3277–3299. doi:10.1016/j.apsb.2023.01.018
61. Tian F, Cai LL, Liu C, et al. Microfluidic technologies for nanoparticle formation. *Lab Chip*. 2022;22(3):512–529. doi:10.1039/d1lc00812a
62. Gimondi S, Ferreira H, Reis RL, et al. Microfluidic devices: a tool for nanoparticle synthesis and performance evaluation. *ACS Nano*. 2023;17(15):14205–14228. doi:10.1021/acsnano.3c01117
63. Fathordoobady F, Sannikova N, Guo YG, et al. Comparing microfluidics and ultrasonication as formulation methods for developing hempseed oil nanoemulsions for oral delivery applications. *Sci Rep*. 2021;11(1):72. doi:10.1038/s41598-020-79161-w
64. Carugo D, Bottaro E, Owen J, et al. Liposome production by microfluidics: potential and limiting factors. *Sci Rep*. 2016;6:25876. doi:10.1038/srep25876
65. Gdowski A, Johnson K, Shah S, et al. Optimization and scale up of microfluidic nanolipomer production method for preclinical and potential clinical trials. *J Nanobiotechnol*. 2018;16(1):12. doi:10.1186/s12951-018-0339-0
66. Mishra V, Heath RJ. Structural and biochemical features of human serum albumin essential for eukaryotic cell culture. *Int J Mol Sci*. 2021;22(16):8411. doi:10.3390/ijms22168411
67. Tanjung YP, Dewi MK, Gatera VA, et al. Factors affecting the synthesis of bovine serum albumin nanoparticles using the desolvation method. *Nanotechnol Sci Appl*. 2024;17:21–40. doi:10.2147/NSA.S441324
68. Victor O, Cheng S, Chaw CS. Desolvation conditions for production of sulfasalazine based albumin nanoparticles: physical properties. *Pharm Front*. 2019;1:e190006. doi:10.20900/pf20190006
69. Bolje A, Gobec S. Analytical techniques for structural characterization of Proteins in solid pharmaceutical forms: an overview. *Pharmaceutics*. 2021;13(4):534. doi:10.3390/pharmaceutics13040534
70. Fan XC, Chen JJ, Shen Q. Docetaxel-nicotinamide complex-loaded nanostructured lipid carriers for transdermal delivery. *Int J Pharm*. 2013;458(2):296–304. doi:10.1016/j.ijpharm.2013.10.036
71. Moreira TDS, Silva ADO, Vasconcelos BRF, et al. DOPE/CHEMS-based EGFR-targeted immunoliposomes for docetaxel delivery: formulation development, physicochemical characterization and biological evaluation on prostate cancer cells. *Pharmaceutics*. 2013;15(3):915. doi:10.3390/pharmaceutics15030915
72. Gao XY, Liu N, Wang ZM, et al. Development and optimization of chitosan nanoparticle-based intranasal vaccine carrier. *Molecules*. 2021;27(1):204. doi:10.3390/molecules27010204
73. Rizvi SSB, Akhtar N, Minhas MU, et al. Synthesis and characterization of carboxymethyl chitosan nanosponges with cyclodextrin blends for drug solubility improvement. *Gels*. 2022;8(1):55. doi:10.3390/gels8010055
74. Galvan-Colorado C, Chanona-Perez JJ, Arredondo-Tamayo B, et al. Obtention of phycobiliprotein nanoparticles from spirulina (Arthrospira maxima) and its characterization by FTIR and microscopic techniques. *Microsc Microanal*. 2023;29:885–888. doi:10.1093/micmic/ozad067.437
75. Eloy JO, Ruiz A, De lima FT, et al. EGFR-targeted immunoliposomes efficiently deliver docetaxel to prostate cancer cells. *Colloids Surf B Biointerfaces*. 2020;194:111185. doi:10.1016/j.colsurfb.2020.111185
76. De Freitas GBL, De Almeida DJ, Carraro E, et al. Formulation, characterization, and in vitro/in vivo studies of capsaicin-loaded albumin nanoparticles. *Mater Sci Eng C Mater Biol Appl*. 2018;93:70–79. doi:10.1016/j.msec.2018.07.064
77. Bronze-Uhle ES, Costa BC, Ximenes VF, et al. Synthetic nanoparticles of bovine serum albumin with entrapped salicylic acid. *Nanotechnol Sci Appl*. 2016;10:11–21. doi:10.2147/NSA.S117018
78. Fang R, Jing H, Chai Z, et al. Study of the physicochemical properties of the BSA: flavonoid nanoparticle. *Eur Food Res Technol*. 2011;233:275–283.
79. Arriagada F, Gunther G, Zabala I, et al. Development and characterization of florfenicol-loaded BSA nanoparticles as controlled release carrier. *AAPS Pharm Sci Tech*. 2019;20(5):202. doi:10.1208/s12249-019-1419-7
80. Fonseca DP, Khalil NM, Mainardes RM. Bovine serum albumin-based nanoparticles containing resveratrol: characterization and antioxidant activity. *J Drug Delivery Sci Technol*. 2017;39:147–155. doi:10.1016/j.jddst.2017.03.017
81. Li Q, Chen F, Liu Y, et al. A novel albumin wrapped nanosuspension of meloxicam to improve inflammation-targeting effects. *Int J Nanomed*. 2018;13:4711–4725. doi:10.2147/IJN.S160714
82. Punam T, Rahul S, Sargar A, et al. Stability study of dosage form: an innovative step. *World J Pharm Res*. 2014;3(2):1031–1050.
83. Aashigari S, Gound R, Sneha S, et al. Stability studies of pharmaceutical products. *World J Pharm Res*. 2019;8:479–492. doi:10.20959/wjpr20191-13872
84. Ren YR, Feng Y, Xu KY, et al. Enhanced bioavailability of dihydrotanshinone I-bovine serum albumin nanoparticles for stroke therapy. *Front Pharmacol*. 2021;12:721988. doi:10.3389/fphar.2021.721988
85. Tartari APS, Mt F, Ziebarth J, et al. Bovine serum albumin nanoparticles enhanced the intranasal bioavailability of silybin in rats. *Pharmaceutics*. 2023;15(12):2648. doi:10.3390/pharmaceutics15122648
86. Younis FA, Saleh SR, El-Rahman SSA, et al. Preparation, physicochemical characterization, and bioactivity evaluation of berberine-entrapped albumin nanoparticles. *Sci Rep*. 2022;12(1):17431. doi:10.1038/s41598-022-21568-8
87. Wang ZL, Li ZW, Zhang D, et al. Development of etopo side-loaded bovine serum albumin nanosuspensions for parenteral delivery. *Drug Deliv*. 2015;22(1):79–85. doi:10.3109/10717544.2013.871600

88. Wei YF, Li LC, Xi YF, et al. Sustained release and enhanced bioavailability of injectable scutellarin-loaded bovine serum albumin nanoparticles. *Int J Pharm*. 2014;476(1–2):142–148. doi:10.1016/j.ijpharm.2014.09.038
89. Amani S, Mahdavi A. pH-responsive hybrid magnetic polyelectrolyte complex based on alginate/BSA as efficient nanocarrier for curcumin encapsulation and delivery. *Int J Biol Macromolecules*. 2019;141:1258–1270. doi:10.1016/j.ijbiomac.2019.09.048
90. Nosrati H, Sharafi A, Danafar H, et al. Bovine serum albumin (BSA) coated iron oxide magnetic nanoparticles as biocompatible carriers for curcumin-anticancer drug. *Bioorg Chem*. 2018;76:501–509. doi:10.1016/j.bioorg.2017.12.033